CFD-based numerical simulation of resistance and propeller open water performance of container ship

Xianmeng Zhang [1, a], Jialin Wang [1, b, *], Xueyuan Jing [1, c], Qinan Zhou [1, d], Haozhe Xue [1, e], Yuting Zhang [1, f]

[1] School of Naval Architecture and Ocean Engineering, Jiangsu University of Science and Technology, Zhenjiang 212100, China.

[a] 1526078940@qq.com, [b, *] 349910872@qq.com, [c] 1751157803@qq.com,

[d] 2870539926@qq.com, [e] 446813474@qq.com, [f] 2086900199@qq.com

Abstract. This paper analyses the resistance characteristics and propeller open water performance of the 108 TEU inland container ship using computational fluid dynamics (CFD). A numerical simulation pool was constructed based on STAR - CCM+, employing a fixed condition and variable parameter approach to simulate and analyse the ship's resistance and propeller performance at various speeds. The CFD technique facilitates the adjustment of both ship speed and inlet speed coefficient, allowing for the calculation of total resistance and the propeller thrust coefficient. Based on the simulation results, a conversion table outlining the actual ship's resistance and the propeller's open-water characteristic curve is established. The findings indicate that the CFD method effectively simulates the ship's drag characteristics and propeller open-water performance, providing valuable insights for evaluating drag and propeller performance in similar vessels.

Keywords: CFD; resistance characteristics; open water performance.

1. Introduction

The numerical simulation of ship hydrodynamics using computational fluid dynamics (CFD) is increasingly favoured in ship research. Its application is becoming more prevalent due to several advantages: its cost-effectiveness, the capability to measure the flow field without contact, and the ability to obtain detailed flow field information. Additionally, CFD eliminates the interference from sensor dimensions and model deformation that can affect the flow field in physical models [1, 2]. At present, scholars have adopted the CFD method to study the hydrodynamic performance of ships. Kong Jinping et al. used ICEM software to establish a three-dimensional propeller model and Fluent software to predict the hydrodynamic performance of the propeller [3]. Qiu Yunming et al. utilised the CFD method to numerically simulate the three-dimensional non-constant viscous flow field experienced during hazardous pairing. They accomplished this by solving the non-constant RANS equations with dynamic mesh technology, using the STAR-CCM+ fluid software to calculate hydrodynamic interactions. The computed values were then compared to relevant experimental data to analyse the transverse forces and yaw moments acting on a stationary ship as it was passed by another vessel moving at speed [4].

With the ongoing deepening of economic globalisation, the demand for inland container transport is on the rise. Consequently, optimising the design of inland container ships is vital for enhancing transport efficiency and minimising energy consumption. This paper centres on the simulation of a 108 TEU river container ship, utilising Computational Fluid Dynamics (CFD) technology to numerically evaluate and forecast the ship's resistance, propulsion performance, and other pertinent parameters. This analysis aims to provide valuable insights into the optimal design of the vessel. By simulating and examining the ship's resistance characteristics under various operational conditions and assessing the propeller's open-water performance, we will compare the CFD simulation results with actual performance data. This comparison not only helps assess the reliability of CFD technology for numerical predictions but also serves as a practical reference for future projects and the optimisation of ship designs, ultimately fostering sustainable and efficient development.

2. CFD basic theory and numerical methods

2.1 Basic Theory

Existing CFD commercial software has the advantages of low cost and short time consumption compared with model experimentation, and the specific flow of numerical solution of CFD is represented by Fig. 1.

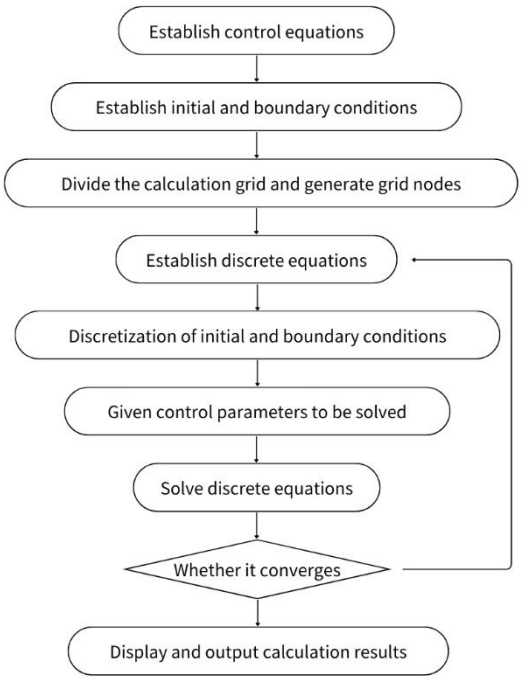

Fig.1 CFD calculation flowchart

2.2 Fluid equations of motion

The laws of physics that govern the motion of a fluid are the laws of conservation of mass and momentum, which are expressed by applying the continuity equation (conservation of mass equation) and N-S equation (conservation of momentum equation) to the above laws of conservation of mass and momentum.

(1) The continuity equation

$$\frac{D\rho}{Dt} + \rho div(v) = 0 \#(1)$$

In this equation, ρ is the fluid density and v is the velocity vector of the flow field.

(2) Momentum conservation equation (Navier-Stokes)

For viscous fluid motion, when the viscosity is a constant, there is the N-S equation

$$\rho \frac{Dv}{Dt} = \rho F_b - gradp + div(2\mu S) + \frac{2}{3} grad(\mu divv) \#(2)$$

In this equation, μ represents the dynamic viscous coefficient, F_b indicates the body force, p denotes the pressure, and S signifies the strain rate tensor. The left side of the equation describes the inertial force per unit volume of the fluid. The first term on the right corresponds to the mass force per unit volume; the second term reflects the pressure gradient force acting on the fluid per unit volume; the third term accounts for viscous deformation stress, and the fourth term represents the expansion stress of the viscous body.

3. Ship resistance calculation

3.1 Ship type parameters

In this paper, a 108 TEU river container ship is selected for numerical simulation analysis, and its ship parameters are shown in Table 1:

Table 1 108TEU River Container Ship Type Parameters

serial number	sports event	parameter value
1	name of ship	108TEU River Container Ship
2	reduction ratio	1:8
3	waterline length	66.00 m
4	Type width (B)	12.76 m
5	Type depth (Z)	3.92 m
6	Bow draft (T_f)	2.78 m
7	Transom draft (T_a)	2.78 m
8	Design speed (V)	13 Km/h
9	Type Drainage Volume (∇)	2090.716 t
10	Wet surface area (S)	1125.8

3.2 Geometric Modeling

Utilising the ship parameters outlined in Table 1, a 3D geometric model of the 108TEU inland container ship has been meticulously crafted in SOLID WORKS, as depicted in Fig. 2. This model has been exported in x.t format and subsequently imported into STAR - CCM+. To ensure a standardised simulation process, the coordinate positions of the simulation model in STAR - CCM+ are described below:

(1) The origin of the simulation coordinate system is the same as the SOLID WORKS file.
(2) X-axis pointing toward the bow
(3) Y-axis toward the port side
(4) The Z-axis is vertically upward

(a) Schematic of the XZ plane (b) Top view

Fig. 2 Comparative view in different directions

3.3 Computational domain and meshing

This simulation employs a numerical pool with a rectangular computational domain. Given the model's symmetry, symmetry planes are established during the computation, ensuring that the computational domain is sufficiently large to minimise the impact of boundary conditions on the results. The configuration of the computational domain is as follows: the bow is located 1.5 times the waterline length (L_{wl}) from the inlet, while the stern is positioned 3.5 L_{wl} from the outlet, resulting in a total length of 6 L_{wl} for the domain. In terms of width, the domain extends 1.5 L_{wl} on each side of the hull, making it 3 L_{wl} wide. In the vertical direction, the domain rises 0.5 L_{wl} above the waterline and extends 1.5 L_{wl} below it. The boundary surfaces of the computational domain are defined by specific angles. The inlet surface and the top of the domain are designated as the velocity inlet, while the outlet is defined as the pressure outlet boundary. The sides are classified as

symmetric boundaries. Since the 108TEU inland waterway container ship is symmetric, the plane of the longitudinal section of the hull is identified as the symmetry plane, with all other surfaces designated as wall surfaces. The final established flow field is illustrated in Fig. 3.

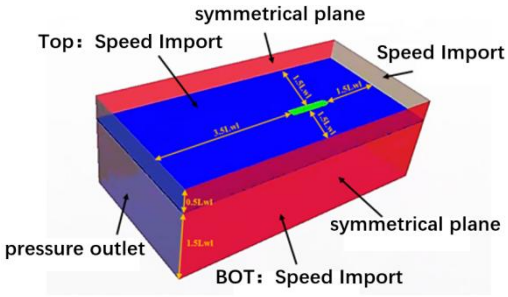

Fig. 3 Computational domain and boundary conditions

The computational domain grid is primarily divided into two sections: the peripheral basin grid and the encrypted area grid surrounding the ship. Utilizing a cut body grid cell generator, local encryption is applied to the ship's hull and the waterline near the surface. This approach results in a total grid count of approximately 2.1 million. The key areas of the ship's hull and the waterline, where local encryption is implemented, are illustrated in Figures 4 and 5.

(a) Stern grid (b) Bow grid

Fig. 4 Schematic diagram of the mesh of the key parts of the hull

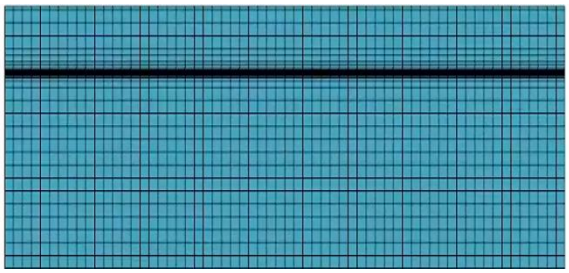

Fig. 5 Free-level mesh encryption

3.4 Numerical simulation results

This paper presents a numerical simulation aimed at predicting the resistance characteristics of 108TEU river container ships at various speeds. The working conditions for calculating ship model resistance have been selected based on the actual operating scenarios of the vessel. The design speed for this ship is set at 13 km/h, and the specified working conditions include speeds of 10 km/h, 11 km/h, 12 km/h, 13 km/h, and 14 km/h. A numerical simulation of the ship model is conducted for these selected conditions to derive resistance values at different speeds. The simulation results are then converted to reflect the resistance of the actual ship, as detailed in Table 2 below.

Table 2 Conversion table for resistance of a real ship

sports event	Vm (m/s)	Vs (km/h)	Rtm (kg)	Ctm	Cfm	Crm	Cfs	Cts	Rts (KN)	Fr	F_D (kg)
1	0.982	10.000	3.060	4.820×10^{-3}	3.104×10^{-3}	1.157×10^{-3}	1.908×10^{-3}	5.550×10^{-3}	22.537	0.109	0.624
2	1.081	11.000	3.646	4.690×10^{-3}	3.052×10^{-3}	1.106×10^{-3}	1.883×10^{-3}	5.430×10^{-3}	28.693	0.120	0.643
3	1.178	12.000	4.359	4.670×10^{-3}	3.007×10^{-3}	1.131×10^{-3}	1.861×10^{-3}	5.409×10^{-3}	31.621	0.131	0.840
4	1.277	13.000	5.203	4.640×10^{-3}	2.965×10^{-3}	1.150×10^{-3}	1.840×10^{-3}	5.379×10^{-3}	36.909	0.142	0.922
5	1.376	14.000	6.185	4.720×10^{-3}	2.927×10^{-3}	1.271×10^{-3}	1.827×10^{-3}	5.456×10^{-3}	41.674	0.153	0.999

The global view of the free surface waveform at different speeds is shown in Fig. 6:

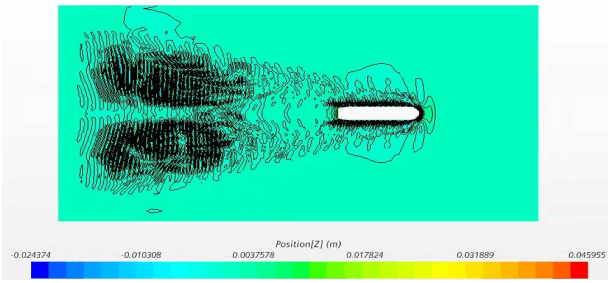

(a) V= 0.982 m/s

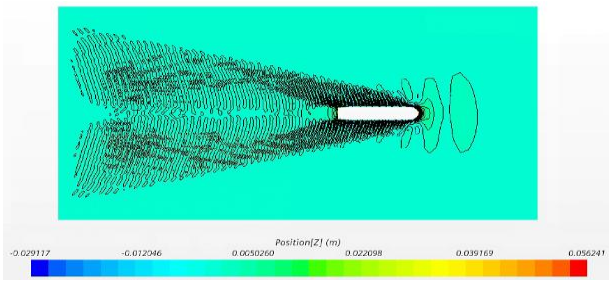

(b) V= 1.0805 m/s

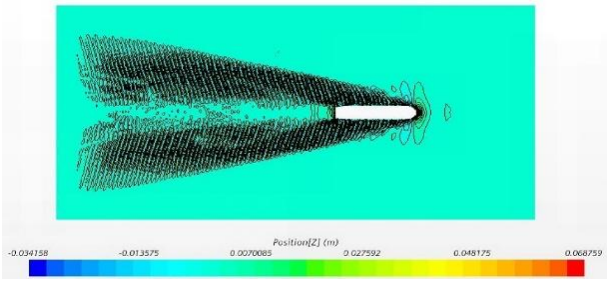

(c) V= 1.178 m/s

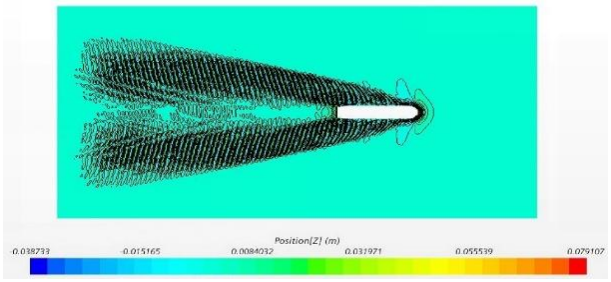

(d) V= 1.277 m/s

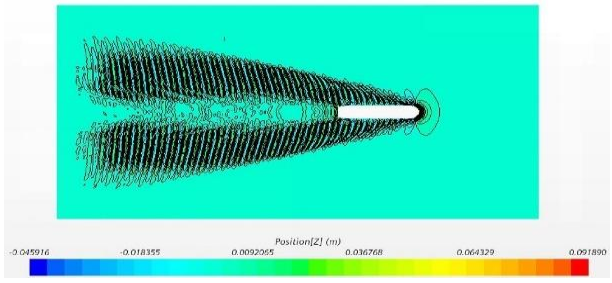

(e) V= 1.376 m/s

Fig. 6 Global view of free surface waveforms at different speeds

The numerical simulation results presented in Table 2 indicate that the total resistance of the ship increases progressively with speed. At lower speeds, such as 10 km/h, the total resistance measures approximately 22.537 kN. As the speed rises to 13 km/h, the total resistance escalates to 41.674 kN. Examining Fig. 6, one can observe distinct differences in the free surface waveforms; at lower speeds, the waveforms are relatively smooth with minor wave heights. However, as the speed increases, the wave heights rise significantly, and the waveforms become increasingly complex. These numerical simulation findings align with the changes in resistance and waveform

characteristics of the ship operating in water under real-world conditions. Consequently, the use of CFD numerical simulation software to analyse the resistance characteristics of the ship proves to be both feasible and accurate, providing valuable insights for subsequent practical applications and ship design optimisation.

4. Propeller open water performance prediction

4.1 Model parameters

In this subsection, the open-water performance of the MAU propeller is evaluated using the CFD software STAR-CCM+ to simulate the flow field within the computational domain by solving the RANS equations. The rotational motion of the propeller is numerically modelled employing the slip mesh technique. The fundamental parameters of the propeller are presented in Table 3.

Table 3 Basic parameters of the propeller

serial number	sports event	Target ships
1	Propeller type	MAU
2	Number of propellers	2
3	Propeller diameter (D_P)	1.7 m
4	Number of paddles	4
5	exchange rate	0.4
6	Pitch ratio (at 0.7 R)	1.08 m
7	Chord length (at 0.7 R)	382.62 mm
8	Maximum thickness (at 0.7 R)	29.07 mm
9	hub-to-diameter ratio	0.14

4.2 Computational setup and meshing

To ensure the comprehensive development of the flow field within the fluid domain while also optimising the use of computational resources and enhancing efficiency, two concentric cylindrical fluid domains are designed around the propeller blade, as illustrated in Fig. 7, Fig. 8 and Fig. 9 below. The inlet of the fluid domain is configured as a velocity inlet, and the outlet is designated as a pressure outlet. The rotating domain of the propeller is treated as a no-slip wall, while the cylindrical surface of the stationary domain is modelled as a symmetric surface. Additionally, the intersection between the cylindrical wall of the rotating domain and the wall of the stationary domain is established to facilitate mass and energy transfer between the two regions. In the numerical simulation, the rotational speed of the propeller remains constant, and the inlet velocity (denoted as V) is varied to achieve different inlet velocity coefficients (J), thus enabling an analysis of the propeller's open-water performance under varying inlet velocity conditions.

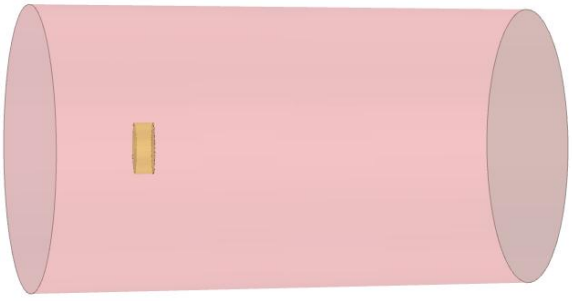

Figure 7 Computational domain

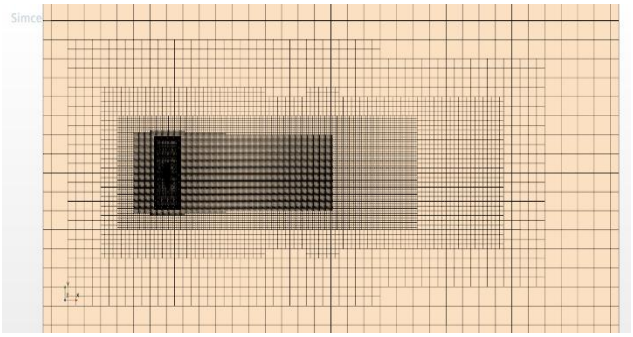

Figure 8 Computational domain grid

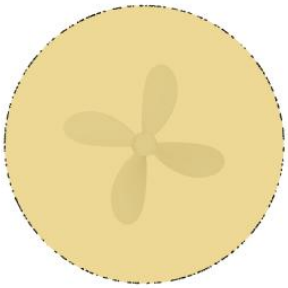

Figure 9 Propeller rotation field

4.3 Numerical simulation results

In this subsection, the numerical simulation evaluates the open water performance of the model paddle within a range of J values from 0.038 to 0.770. The average thrust and torque coefficients for one complete rotation cycle are identified as the results corresponding to the current operating point. For these calculations, the SST k-ω turbulence model has been selected, as it effectively accounts for the transport characteristics of turbulent shear, making it particularly well-suited for simulating the complex flow field around the surface of the paddle.

Based on the numerical simulation data obtained after the open water test of the propeller, the calculated parameters of the open water characteristics and the parameters after smoothing are shown in Table 4 below.

Table 4 Open water characterisation parameters

serial number		raw data			smooth handling		
	Feed rate coefficient	coefficient of thrust	torque coefficient	Advancing efficiency	thrust ratio	torque coefficient	impel efficiency
	J	K_T	$10K_Q$	η_0	K_T	$10K_Q$	η_0
1	0.038	0.194	0.206	0.055	0.192	0.208	0.055
2	0.075	0.197	0.211	0.110	0.196	0.212	0.11
3	0.148	0.192	0.219	0.210	0.198	0.217	0.215
4	0.221	0.191	0.212	0.313	0.189	0.212	0.314
5	0.295	0.175	0.204	0.402	0.173	0.202	0.402
6	0.369	0.155	0.190	0.476	0.153	0.188	0.476
7	0.442	0.138	0.182	0.528	0.136	0.181	0.53
8	0.480	0.118	0.165	0.560	0.118	0.161	0.56
9	0.517	0.102	0.147	0.576	0.105	0.149	0.576
10	0.554	0.094	0.136	0.586	0.091	0.138	0.585
11	0.591	0.077	0.124	0.583	0.077	0.125	0.583
12	0.638	0.059	0.109	0.556	0.059	0.107	0.557
13	0.676	0.043	0.095	0.503	0.043	0.092	0.504
14	0.714	0.026	0.076	0.395	0.026	0.076	0.395
15	0.751	0.009	0.058	0.190	0.009	0.058	0.191
16	0.770	0.001	0.048	0.006	0.001	0.048	0.006

The surface pressure distribution of the propeller blade at different speeds is shown in Fig. 10 below:

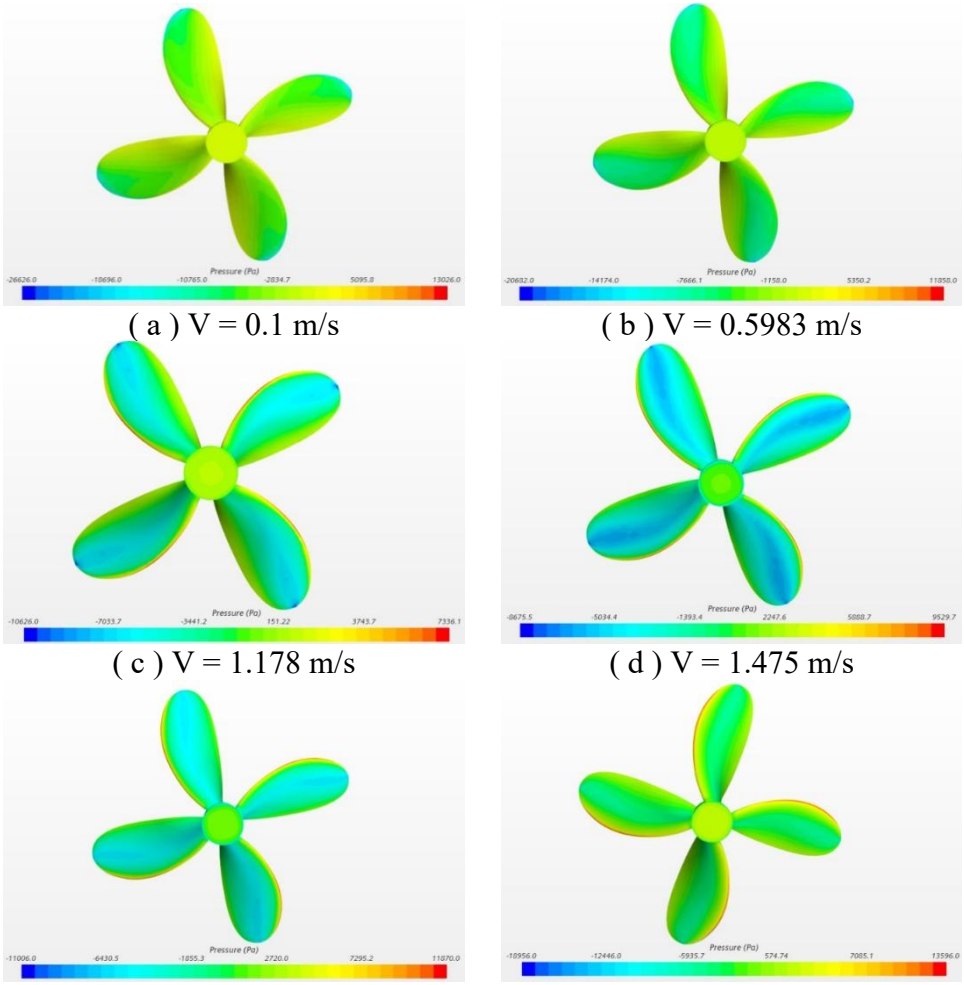

(a) V = 0.1 m/s (b) V = 0.5983 m/s

(c) V = 1.178 m/s (d) V = 1.475 m/s

(e) V= 1.8 m/s (f) V = 2.05 m/s

Fig. 10 Surface pressure distribution

Based on the data from CFD numerical simulation, the open water behaviour curve of the paddle mould and the open water behaviour and load curve of the propeller are plotted as shown in Fig. 11 and Fig. 12 below.

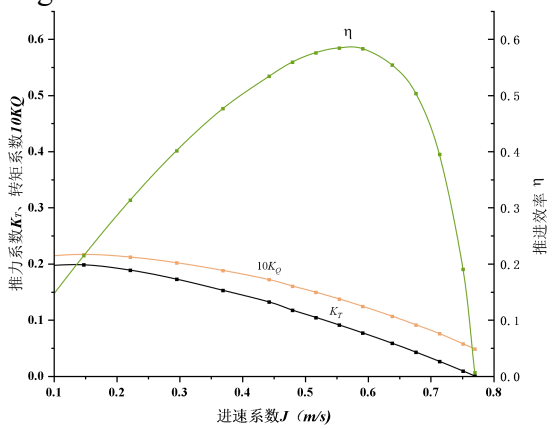

Figure 11 Open Water Characterization Curve

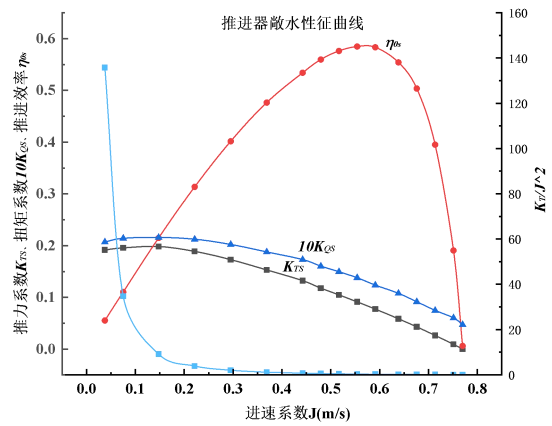

Figure 12 Open Water Characterization and Load Curves

In the actual open-water experiment, when the rotational speed of the propeller is kept constant, the experimental results demonstrate an increase in the inlet velocity coefficient, J, alongside a decrease in the thrust coefficient, K_T. Based on the open-water parameters derived from numerical simulations of propeller performance using CFD software, Table 4 indicates that the thrust

coefficient of the numerically simulated propeller diminishes progressively as the inlet velocity coefficient increases at the same rotational speed. This observation aligns with the typical characteristics of propeller hydrodynamics. Consequently, utilising CFD software to analyse the open-water performance of the propeller is indeed feasible, offering a valuable technical reference for enhancing the design of ship propulsion systems in practical applications.

5. Summary

This paper utilises Computational Fluid Dynamics (CFD) technology to numerically simulate the drag characteristics and open water performance of the MAU propeller for the 108TEU river container ship. A three-dimensional geometric model and a structured mesh are created, setting multistage speeds (10 ~ 14 km/h) and speed coefficients (J = 0.038 ~ 0.770) to effectively simulate the ship's drag characteristics and the propeller's open water performance. The total resistance of the ship significantly increases with rising speed, and the propeller thrust coefficient shows a decreasing trend as the inlet speed coefficient rises. The simulation results align with the observed trends of the ship's drag force and the hydrodynamic characteristics of the propeller during actual voyages, thereby validating the reliability of CFD technology. This study provides a valuable simulation reference for further investigations into the drag force characteristics of similar vessels and the evaluation of propeller performance in open water.

References

[1] GUO Haiqiang, ZHU Renchuan, MU Guoping, et al. Testing and analysing technology of ship hydrodynamic coefficient in numerical wave pool[J]. China Shipbuilding,2008,49(S1):58-65.

[2] ZHU Renchuan, GUO Haiqiang, MU Guoping, et al. A calculation method of additional mass and damping of ships based on CFD theory[J]. Journal of Shanghai Jiao Tong University,2009,43(02):198-203.DOI:10.16183/j.cnki.jsjtu.2009.02.009.

[3] KONG Jinping, WU Botao, KONG Lingzhi. Hydrodynamic performance analysis of ship dual propeller based on CFD[J]. Ship Science and Technology,2019,41(05):37-41.

[4] QIU Yunming, LU Dongqing, Deng Rui. Numerical study of hydrodynamics during ship hazardous pair encounter[J]. Ship Science and Technology,2020,42(09):76-80+102.